

# The Active Atlas: Combining 3D Anatomical Models with Texture Detectors

Yuncong Chen<sup>1</sup>, Lauren McElvain<sup>2</sup>, Alexander Tolpygo<sup>3</sup>, Daniel Ferrante<sup>3</sup>, Harvey Karten<sup>2</sup>, David Kleinfeld<sup>2</sup>, Yoav Freund<sup>1</sup>

<sup>1</sup> Department of Computer Science and Engineering, University of California, San Diego

<sup>2</sup> Department of Physics, University of California, San Diego

<sup>3</sup> Cold Spring Harbor Laboratory

**Abstract** While modern imaging technologies such as fMRI have opened exciting new possibilities for studying the brain in vivo, histological sections remain the best way to study the anatomy of the brain at the level of single neurons. The histological atlas changed little since 1909 and localizing brain regions is a still a labor intensive process performed only by experienced neuro-anatomists. Existing digital atlases such as the Allen Brain atlas are limited to low resolution images which cannot identify the detailed structure of the neurons.

We have developed a digital atlas methodology that combines information about the 3D organization of the brain and the detailed texture of neurons in different structures. Using the methodology we developed an atlas for the mouse brain-stem and mid-brain, two regions for which there are currently no good atlases. Our atlas is “active” in that it can be used to automatically align a histological stack to the atlas, thus reducing the work of the neuroanatomist.

**Keywords:** Brain, Atlas, Texture, Registration, Localization, Confidence, significance

## 1 Introduction

The modern approach to mapping distinct brain regions was pioneered by Korbinian Brodmann in 1909 [3] and relied on visual recognition of cytoarchitectural features in brain sections. Several paper atlases have been created for the brains of different species [10].

The primary methods for expert annotation of brain regions have changed little since 1909: typically, localizing brain regions is a labor intensive process performed by an experienced neuro-anatomist, possibly with the aid of a published atlas. We propose a machine-learning approach for atlas construction that makes use of the texture recognition of brain cytoarchitectonics, to immitate human pattern recognition.

There are several modern digital brain atlases designed specifically for brain sections that utilize image recognition algorithms. The best known are the Allen Reference Atlas for mouse [1, 4, 6] and the Zilles Atlas for rat [14]. A commonality to these two atlases is that they are based on low resolution images ( $64\mu\text{m}$  for Zilles,  $50\mu\text{m}$  for Allen). At this resolution registration can be perfrmed by finding the transformation with the highest correlation.

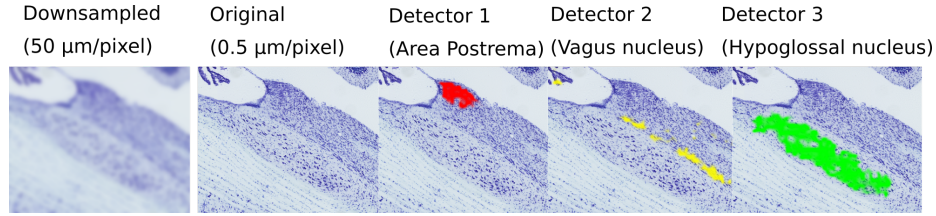


**Figure 1. A demonstration of the limitation of reduced resolution brain images** The “original” image was taken at 0.5  $\mu\text{m}/\text{pixel}$ . The three images “Detector 1,2,3” represent the detection of known brain structures based on their texture. The “Downsampled” image lacks the high-resolution details needed to distinguish the structure.

The problem is that at this resolution the cytoarchitectonics texture of brain regions cannot be identified, which results in poor localization in brain regions that lack high contrast boundaries. In this work our focus is on the mouse brainstem, which lack high contrast boundaries. To overcome this limitation we have developed a texture-based atlas we call the *active atlas*. (see Figure 1). This atlas operates on the full-resolution images and uses texture detectors to distinguish between structures that cannot be identified in low resolution images. This distinguishes our approach from atlases based on MRI or optical volumes [8,9,11,13].

The contributions of this work are:

- Detection of cytoarchitectonics textures that are visible only at high magnification.
- Detection of discrete structures, as opposed to a global registration.
- Characterization of the variation in the relative locations of the brain structures.
- The use of iterative refinement to reduce the human annotation.

The paper is organized as follows. Section 2 describes the procedure for building an active atlas. Section 3 presents evaluation results that demonstrate the confidence of registration and accuracy of texture detection.

## 2 The Active Atlas

The active atlas consists of two parts:

1. **Anatomical model:** stores for each of 28 structures in the brainstem, the position statistics and probabilistic shape.
2. **Texture classifiers:** predict the probability that a given image patch corresponds to a particular structure.

The construction of the atlas is iterative, starting with a initialization step that required significant labor of an experienced neuroanatomist, followed by refinement steps which require little or no expert labor (see Figure 2).

In our case, the initial step was to annotate 3 stacks of mouse brainstem, which required 30 hours of work of an experienced neuroanatomist.

From these three annotated stacks, and initial anatomical model and a set of texture classifiers was constructed.

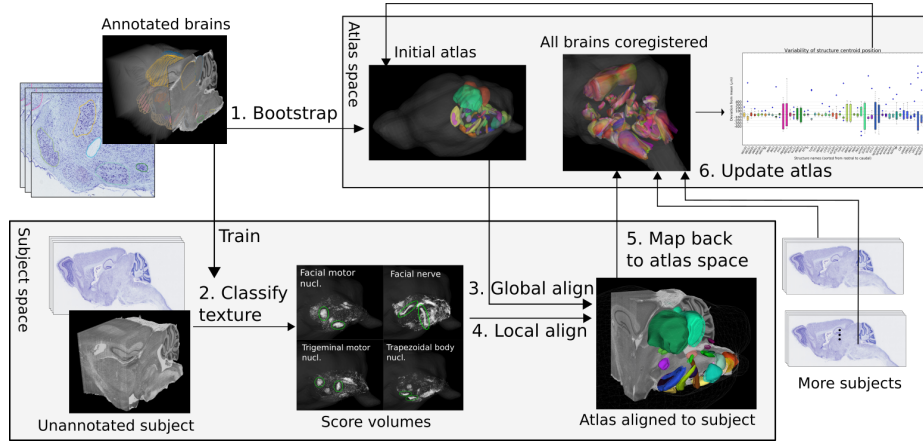


**Figure 2.** Incremental atlas building workflow

The refinement was performed using nine additional stacks which were *not* annotated. These stacks were aligned to the initial atlas and the information from this alignment was used to refine the atlas and to estimate the variability of the atlas parameters from brain to brain.

We provide more detail on each of the construction steps in the subsections below.

## 2.1 Preprocessing

Our dataset consist of sagittal brain sections from twelve mice of the same strain and age. The  $20\mu m$  sections are mounted with a tape transfer system [12] to ensure minimal distortion. Each specimen gives roughly 400 sections. They are stained with Nissl and scanned at  $0.5\mu m$  resolution, demonstrating clear cytoarchitectonic features. For each stack, the sections are registered via in-plane rigid transforms. This allows reconstruction of a 3D volume for each specimen by stacking up the aligned images (see “Unannotated subject” in Figure 2).

## 2.2 Estimation of Anatomical model

Model estimation takes as input a current model (initially null) and a set of annotated brains. It produces as output a new anatomical model that is more accurate than the original.

Estimation of the anatomical model consists of two steps: position estimation and shape estimation, which we describe below:

**2.2.1 Position estimation** For each structure we define a *centroid*. The relative position of a structure is the position of it’s centroid. In order to define the average positions, the stacks are co-registered in a common space. We exploit the saggital (left-right) symmetry of the brain. First, the mid-saggittal plane of every specimen is estimated by fitting the middle points of paired structures. Then all specimens are registered using 3D affine transforms with the constraint that all mid-saggital planes must coincide. The new positions of the same structure in the common space are used to derive an average

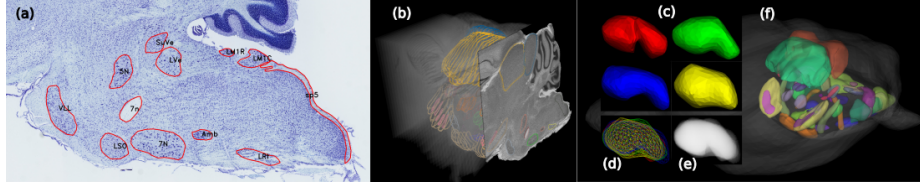


**Figure 3.** (a) Manually drawn structure boundaries (b) Aligned boundary series in 3D (c) Same structure from different hemisphere and different brains (d) Aligned mesh (e) Probabilistic average shape (f) Anatomical reference model

position, such that the average positions of all paired structures are symmetric with respect to the mid-sagittal plane. In addition, the  $3 \times 3$  covariance matrix of the positions, denoted  $C$ , is included in the atlas. This matrix will be used to improve the alignment of future stacks, and is of interest to anatomist when they study brain structure variability.

**2.2.1 Shape estimation** By interpolating aligned boundary series, we reconstruct a 3D mesh for every structure. Meshes of the same structure from both hemispheres and all annotated brains are aligned using the Iterative Closest Point (ICP) algorithm [2]. The aligned meshes are converted to volumes and a probabilistic mean volume is computed by voxel-voting, where each voxel is assigned a probability according to the percentage of volumes covering it (Figure 3). We use the notation  $\mathbf{a}(\mathbf{p})$  to denote the probability vector that is associated with voxel at location  $\mathbf{p}$ .

### 2.3 Learning Texture Classifiers

The purpose of texture classifiers is to differentiate a structure from its surrounding area. Image patches roughly  $100\mu\text{m}$  by  $100\mu\text{m}$  are used as input. For each structure, a binary logistic regression classifier is trained using a positive set of patches extracted from the interior of the structure boundaries and a negative set extracted from the surrounding region within  $50\mu\text{m}$  from the boundaries.

We train each texture classifier to discriminate a structure from its immediate surrounding. We found that this gives better results than training against the entire background. The probable reason is that the anatomical atlas constrains the approximate position of most of the structures so the main task of the texture classifier is to identify small errors in the location of the structure.

The feature vectors given as input to the texture classifiers are the 1024-dimensional output of a pre-trained deep convolutional neural network (Inception-BN [7]). Although the network was originally trained for classifying natural images, it proves also effective for classifying histology textures.

For an unannotated image, these classifiers are applied to patches on a regular grid with  $25\mu\text{m}$  spacing. Sparse scores generated by each classifier over the entire image are interpolated to form a dense score map. Score maps for all images of a specimen are stacked according to the previously computed intra-stack transforms to form a set of 3D score volumes. Each score volume represents a probabilistic estimate for the 3D positions of a particular structure in the specimen (Figure 4).

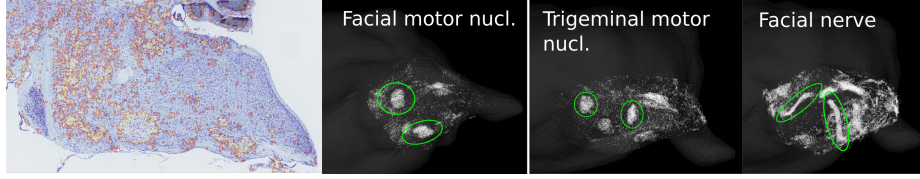


**Figure 4.** (a) A example score map of facial motor nucleus (b) Stacking 2D maps forms the score volume of this structure. (c,d) Score volumes of other structures.



**Figure 5.** (a) Reference model globally registered to the specimen. (b) Global registration. Showing the structure contours on a section. Structures are roughly aligned. (c) Local registration. Structures are aligned perfectly.

## 2.4 Registering Atlas to Specimen

Registration is driven by maximizing the sum of the dot products between the score vectors of the specimen volume and the probability vectors of the atlas volume at all voxels. A global transform first aligns the atlas roughly with the whole specimen. 3D affine transform is used to account for non-vertical cutting angle and scale change due to dehydration. Separate local transforms are then applied to each structure so independent variations can be captured. We now give a precise definition of the way the total score.

Let  $\Omega$  be the set of voxels of the anatomical atlas and denote by  $\mathbf{p}$  the voxel at a particular location. Let  $\mathbf{a}(\mathbf{p})$  be the probability distribution over the structures at the voxel  $\mathbf{p}$ . Let  $\mathbf{s}(\mathbf{p})$  be the score vector that consists of the texture scores for each of the structures. The 3D affine transform  $T$  maps a voxel  $\mathbf{p}$  from the atlas volume to a voxel  $T(\mathbf{p})$  in the specimen volume.  $T(\mathbf{p}) = L\mathbf{p} + \mathbf{t}$ , where  $L \in \mathbb{R}^{3 \times 3}$  defines the linear transformation and  $\mathbf{t} \in \mathbb{R}^3$  defines the translation.

For the global transform, the objective is to maximize  $F(T) = \sum_{\mathbf{p} \in \Omega} \mathbf{a}(\mathbf{p}) \cdot \mathbf{s}(T(\mathbf{p}))$  where  $\Omega$  is the set of all nonzero voxels in the atlas volume.

For local transform, only the voxels  $\Omega_k$  in and around the particular structure  $k$  are concerned, and the only allowed transformation is translation.

$$F(T) = \sum_{\mathbf{p} \in \Omega_k} \mathbf{a}(\mathbf{p}) \cdot \mathbf{s}(\mathbf{p} + \mathbf{t}) - \eta \mathbf{t}^T C \mathbf{t},$$

where  $\mathbf{t}$  is the translation. The extra regularization term penalizes local deviation from the atlas-defined position, where  $C$  is the inverse of the location covariance matrix computed in section 2.2.1 in the atlas. Optimization starts with grid search over the translation parameters, followed by gradient descent where the learning rate is adapted using Adagrad [5]. (Figure 5)

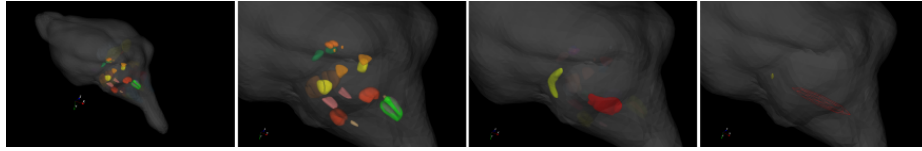


**Figure 6.** (a, b) Confident structures (c) Two unconfident structures (d) Uncertainty ellipsoids. The elongated structure VLL (yellow) is uncertain only in its axial direction, while Sp5I (red) is uncertain in rostral-caudal direction because its rostral and caudal boundaries are ambiguous.

## 2.5 Evaluating Registration Confidence

The registration algorithm seeks a local maxima of the objective function  $F(T)$ . We quantify the confidence of the registration by considering the height and the width of the local maxima. The height of the peak is normalized by considering a  $z$ -test relative to the variance within a sphere around the peak. The width is computed as the Hessian of the  $z$ -score around the peak. Large values in the Hessian correspond to a sharp peak and to highly accurate localization.

A confidently registered structure must also be within the stored variability limits for it to be automatically incorporated into the atlas; otherwise the update must be approved by a human reviewer. For unconfident registrations, the direction corresponding to the smallest eigenvalue is prioritized for correction by reviewer. For example, the reviewer needs to only move an elongated structure along the axial direction if the structure is confident with its lateral position. (Figure 6)

## 2.6 Update Atlas

After registrations are reviewed, Bootstrap step is repeated to derive new average shapes and position statistics. Additional training patches can also be collected to improve the classifiers.

# 3 Results

## 3.1 Confidence of Registrations

The global registrations across all specimens have an average  $z$ -score of 2.06. The average peak radius is  $98\mu m$  in the steepest direction and  $123\mu m$  in the flattest direction. This suggests that the derived reference model captures the common anatomy of this population and matches all specimens with little space for adjustment. Figure 7 and 8 show these for the local registrations of each structure. The average  $z$ -score is 1.79, and the peak radius is between  $90\mu m$  and  $250\mu m$  for most structures. Generally, small structures tend to be registered more confidently than large ones.

## 3.2 Variability of Structure Position

Variability in structure position is captured by the translation components of the local transforms estimated for each structure. Figure 9 shows structure variability across all

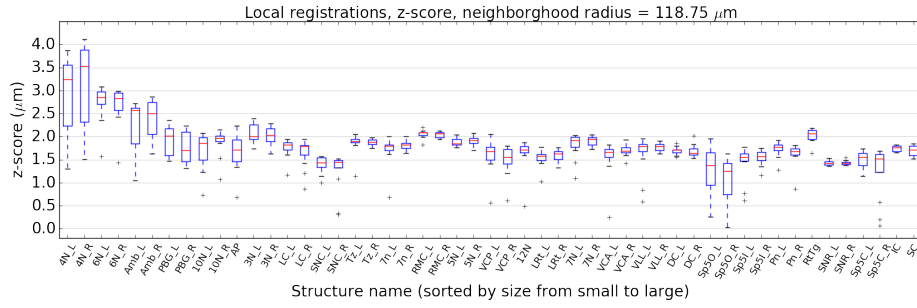


**Figure 7.** Average z-scores of the local registrations of different structures.

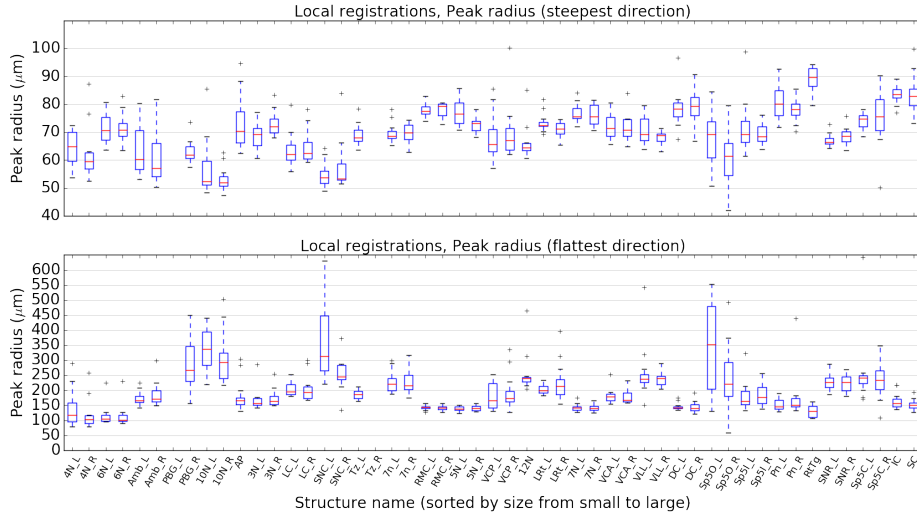


**Figure 8.** Average peak radius of the local registrations of different structures.

specimens. Most structures vary within 100 $\mu\text{m}$  of the atlas mean position. Some structures are particularly variable. They are also the ones whose boundaries are difficult to define. The same structure in left and right hemispheres generally have similar variability.

### 3.3 Accuracy of Texture Classifiers

The classifiers generated by bootstrapping are tested using a new set of patches collected from the annotated specimens in the same ways as the training set. Negative examples are extracted from the surrounding region of a structure because only the accuracy near the structure is of interest. Figure 10 shows the accuracies for different structures averaged over all specimens. They range from 0.7 to 0.9 with a mean of 0.79. Larger structures tend to be harder to classify possibly due to their texture being more inhomogeneous.



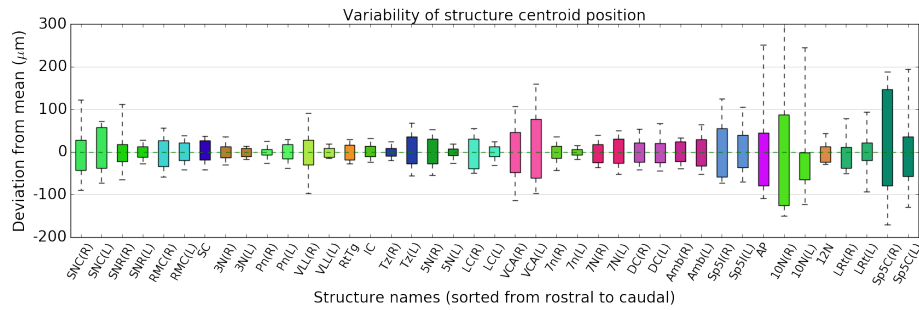


**Figure 9.** Variability of structure centroid positions. Same color indicates the same structure in left and right hemispheres.

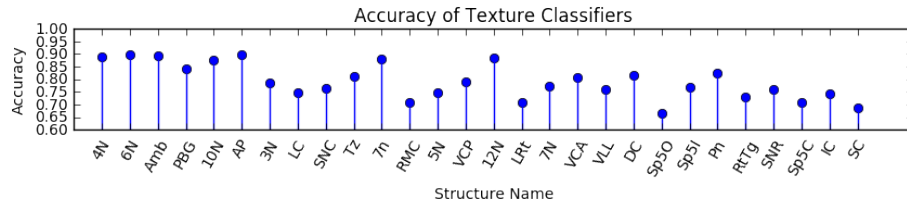


**Figure 10.** Accuracy of texture classifiers. (Structures sorted by increasing size)

## 4 Conclusion

The results demonstrate a form of co-training between the anatomical model and the texture classifiers. On the one hand, registrations perform well despite the classifiers for some structures are suboptimal, due to the strong constraint by the anatomical model. On the other hand, confident detection of the characteristic textures of many structures allows specimen-specific deviations from the current anatomical model to be discovered, contributing to more accurate variability. The synergy between the anatomical information and textural information is the key feature of the proposed active atlas.

## References

1. Technical white paper: Allen mouse common coordinate framework. Tech. rep. (2015) [1](#)
2. Besl, P.J., McKay, N.D.: Method for registration of 3-d shapes. In: Robotics-DL tentative. pp. 586–606. International Society for Optics and Photonics (1992) [2.2](#)
3. Brodmann, K., Garey, L.: Brodmann's: Localisation in the Cerebral Cortex. Springer (2006) [1](#)
4. Dong, H.: Allen Reference Atlas: a digital color brain atlas of the C57BL/6J male mouse. John Wiley & Sons (2008) [1](#)
5. Duchi, J., Hazan, E., Singer, Y.: Adaptive subgradient methods for online learning and stochastic optimization. JMLR 12(Jul), 2121–2159 (2011) [2.4](#)
6. Fonov, V., et al.: Unbiased average age-appropriate atlases for pediatric studies. Neuroimage 54(1), 313–327 (2011) [1](#)



7. Ioffe, S., Szegedy, C.: Batch normalization: Accelerating deep network training by reducing internal covariate shift. arXiv preprint arXiv:1502.03167 (2015) [2.3](#)
8. Johnson, G.A., et al.: Waxholm space: an image-based reference for coordinating mouse brain research. *Neuroimage* 53(2), 365–372 (2010) [1](#)
9. Mazziotta, J., Toga, A., et al.: A probabilistic atlas and reference system for the human brain: International consortium for brain mapping (icbm). *Philosophical Transactions of the Royal Society of London B: Biological Sciences* 356(1412), 1293–1322 (2001) [1](#)
10. Paxinos, G., Franklin, K.B.: *The mouse brain in stereotaxic coordinates*. Gulf Professional Publishing (2004) [1](#)
11. Peng, H., et al.: Brainaligner: 3d registration atlases of drosophila brains. *Nature methods* 8(6), 493–498 (2011) [1](#)
12. Pinskiy, V., Jones, J., Tolpygo, A.S., Franciotti, N., Weber, K., Mitra, P.P.: High-throughput method of whole-brain sectioning, using the tape-transfer technique. *PLoS ONE* 10(7) (2015) [2.1](#)
13. Ronneberger, O., et al.: Vibe-z: a framework for 3d virtual colocalization analysis in zebrafish larval brains. *Nature Methods* 9(7), 735–742 (2012) [1](#)
14. Zilles, K.: *The Cortex of the Rat: A Stereotaxic Atlas*. Springer Berlin Heidelberg (1985) [1](#)